AECL-6412

ATOMIC ENERGY OF CANADA LIMITED

L'ÉNERGIE ATOMIQUE DU CANADA LIMITÉE

NIRVANA, A HIGH-TEMPERATURE CREEP MODEL FOR ZIRCALOY FUEL SHEATHING

NIRVANA
Modèle de fluage à haute température des gaines en Zircaloy destinées au combustible nucléaire

H.E. SILLS and R.A. HOLT

Chalk River Nuclear Laboratories Laboratoires nucléaires de Chalk River

Chalk River, Ontario

May 1979 mai

ATOMIC ENERGY OF CANADA LIMITED

NIRVANA,
A HIGH-TEMPERATURE CREEP MODEL FOR ZIRCALOY FUEL SHEATHING

by

H.E. Sills and R.A. Holt

Applied Mathematics Branch
Chalk River Nuclear Laboratories
Chalk River, Ontario

May 1979

AECL-6412

NIRVANA

Modèle de fluage à haute température des gaines en Zircaloy destinées au combustible nucléaire

par

H.E. Sills et R.A. Holt

Récumé

On a développé un modèle à composants multiples pour décrire la déformation plastique temporaire des gaines en Zircaloy lors des élévations transitoires de température. A partir de cartes de déformation, on identifie trois mécanismes de déformation se produisant en principe dans les trois champs phasiques du Zircaloy (α, $\alpha+\beta$, β) - fluage diffusionnel, fluage de dislocation et contrainte athermique. Un composant de contrainte se produisant durant la transformation $\alpha \rightarrow \beta$ est également identifié. On tient compte des changements microstructurels qui modifient les taux de déformation: structure des grains; recristallisation; transformation des phases. Les composants individuels du modèle représentent les phénomènes métallurgiques connus. Le modèle combiné est en excellent accord avec les données d'essais transitoires allant de 700 à 1600 K, dans une gamme de taux de chauffage allant de 0 à 100 K/s et dans une gamme de taux de contrainte allant de 10^{-5} à $10^{-1}.s^{-1}$.

Pour qu'une comparaison avec les données disponibles soit possible, le modèle de fluage transitoire a été combiné avec la représentation d'un tube axialement uniforme à paroi mince ayant les propriétés d'une matière anisotropique. NIRVANA, le code machine qui en résulte donne la possibilité de simuler des essais de tubes uniaxiaux et biaxiaux dans des gammes spécifiques de contraintes et de températures.

L'Energie Atomique du Canada, Limitée
Laboratoires nucléaires de Chalk River
Chalk River, Ontario

Mai 1979

AECL-6412

ATOMIC ENERGY OF CANADA LIMITED

NIRVANA, A HIGH-TEMPERATURE CREEP MODEL FOR ZIRCALOY FUEL SHEATHING

by

H.E. Sills and R.A. Holt

ABSTRACT

We have developed a multi-component model to describe the transient plastic deformation of Zircaloy fuel sheathing during high-temperature transients. From deformation maps, we identify three deformation mechanisms, which in principle, occur in all three phase fields of Zircaloy (α, $\alpha+\beta$, β) - diffusional creep, dislocation creep and athermal strain. A strain component occurring during the $\alpha \rightarrow \beta$ transformation is also identified. Microstructural changes which alter deformation rates - grain structure, recrystallization, phase transformation - are accounted for. The individual components of the model represent known metallurgical phenomena. The combined model gives excellent agreement with transient test data from 700 - 1600 K, a range of heating rates from 0 - 100 K/s and a range of strain rates from 10^{-5} - $10^{-1} \cdot s^{-1}$.

To enable comparison with available data, the transient creep model was combined with an axially uniform, thin-walled tube representation having anisotropic material properties. The resulting computer code, NIRVANA, provides facilities for simulating uniaxial and biaxial tube tests over specified stress/temperature histories.

Applied Mathematics Branch
Chalk River Nuclear Laboratories
Chalk River, Ontario

May 1979

AECL-6412

NIRVANA,
A HIGH-TEMPERATURE CREEP MODEL FOR ZIRCALOY FUEL SHEATING

by

H.E. Sills and R.A. Holt

1. INTRODUCTION

To allow the large number of experiments on the high-temperature deformation of Zircaloy tubing [1-11] to be analyzed, a transient creep model has been coupled with a thin-walled fuel sheath representation. The resulting computer program, NIRVANA, provides a detailed simulation of the deformation of axially uniform Zircaloy tubes at elevated temperature (>700 K).

High-temperature transients would expose the Zircaloy sheath to rapid and non-linear stress/temperature changes. Such environmental variations produce time dependent changes in grain size, anisotropy, dislocation structure and phase distribution which interact strongly with the high-temperature creep deformation. The creep model of Sills and Holt [12] represents these transient changes in microstructure.

Steady-state creep models represent the large strain (rupture) behaviour of pressurized tubes. However, at low plastic strain levels (<10%) transient effects occur which must be accounted for to evaluate deformations accurately. As steady-state creep is a special case of transient creep, the NIRVANA transient creep model represents the full range of strain behaviour.

NIRVANA provides different modes of execution so that simulations involving either uniaxial or biaxial stresses and transient or constant temperatures can be performed. Wherever possible, the creep model has been verified using data sources independent from those used to calibrate the model.

2. TUBE MODEL

The Zircaloy sheath is a thin-walled tube. For biaxial stress simulations, the tube has closed ends. The anisotropy of material properties is represented using Hill's plasticity theory for anisotropic materials [13]. The equivalent stress (σ_e) is defined by the expression

$$\sigma_e^2 = F(\sigma_\theta-\sigma_z)^2 + G(\sigma_z-\sigma_r)^2 + H(\sigma_r-\sigma_\theta)^2 \qquad \ldots 1$$

in which F, G, and H are anisotropic factors, the σ_i are principal stresses and the subscripts θ, r and z refer to tangential, radial and axial directions respectively. The anisotropic factors are experimentally determined and typical values for Zircaloy sheathing material are given in the following table.

TABLE 1 VALUES OF ANISOTROPY VALUES FOR ZIRCALOY SHEATH

Condition	F	G	H
As-received	0.773	0.532	0.195
α-annealed	0.956	0.322	0.222
β-annealed	0.572	0.418	0.510
β -phase	0.5	0.5	0.5

For biaxial tube tests (closed-end, pressurized), the principal stresses are defined as

$$\sigma_\theta = \frac{r}{t} P, \quad \sigma_z = \frac{\sigma_\theta}{2}, \quad \sigma_r = 0 \qquad \ldots 2$$

In uniaxial tests, the principal stresses are defined as

$$\sigma_z = L/A, \quad \sigma_\theta = \sigma_r = 0 \qquad .. 3$$

where the parameters are differential pressure (P), mean sheath radius (r), sheath wall thickness (t), axial load (L) and tube cross-sectional area (A).

After selecting the mode of execution in NIRVANA (uniaxial/biaxial), the stress state is calculated from the boundary conditions. This stress state (σ_e) is then used with the creep model to find the equivalent creep rate.

3. TRANSIENT CREEP MODEL

The microstructural transient creep model of Sills and Holt [12] is used to describe the high temperature creep behaviour of the Zircaloy sheathing. A stress/temperature transient may

cause significant changes in the grain size, dislocation density and phase distribution of Zircaloy. These microstructural changes occur continuously and have a strong effect on the creep behaviour. As the sheath microstructure is accounted for by the model, manufacturing differences which affect anisotropy, grain size and dislocation structure can be explicitly represented.

3.1 Creep Models

Creep processes in the model include thermal dislocation creep, athermal dislocation glide, diffusion creep (grain boundary sliding) and phase transition strain.

The total creep rate is determined by adding the separate creep components as suggested by Ashby [14]. However, domains of stress and temperature can be displayed in which one of the creep components is dominant (Figure 1).

3.1.1 *Dislocation Creep, $\dot{\varepsilon}_d$ and Athermal Glide $\dot{\varepsilon}_a$*

During transient creep, the dislocation density in the sheath changes continuously. During strain, dislocations are produced (work hardening). As the dislocation density increases, dislocations are thermally annihilated (recovery). The rate of change of dislocation density at any time is determined by the competition between the work hardening rate and the recovery rate. The presence of dislocations is represented by an internal stress field which must be overcome by an applied stress before creep occurs. The effective stress (σ_*) is defined as the difference between the applied stress (σ_a) and the internal stress (σ_i).

$$\sigma_* = \sigma_a - \sigma_i \qquad \ldots 4$$

It is this effective stress which is responsible for dislocation creep and athermal glide.

The rate of change of internal stress is†

$$\dot{\sigma}_i = W\text{-}R = A\dot{\varepsilon}_d - \frac{A\dot{\varepsilon}_d}{C} \exp\left(\frac{-Q}{T}\right) \sigma_*^{\,m}\, \sigma_i \qquad \ldots 5$$

where W is the work hardening rate and R is the recovery rate. The expression for the dislocation creep is

$$\dot{\varepsilon}_d = \dot{\varepsilon}_o \exp\left(\frac{-Q}{T}\right) \sigma_*^{\,n} \qquad \ldots 6$$

†A dot indicates the derivative of a variable with respect to time e.g. $\dot{\sigma}_i = d\sigma_i/dt$.

Values of the constants of equations 5 and 6 are given in table 2.

TABLE 2: Constants for Equations 5 and 6 for $\dot{\varepsilon}$ in s^{-1}, T in K and σ in Mpa

Constant	α-phase	β-phase
A	0.016E*	24.75
C	0.33	0.29
m	4.3	3.1
$\dot{\varepsilon}_o$	1.88×10^4	7.1
Q	34726	15702
n	5.3	3.6

*E = Young's modulus.

When $\sigma_i = \sigma_i^{ss}$, $\dot{\sigma}_i = 0$ and the material displays steady state creep. When $\sigma_i < \sigma_i^{ss}$, $\dot{\sigma}_i$ is positive, σ^* decreases at constant σ_a, and normal primary creep occurs (16). When $\sigma_i > \sigma_i^{ss}$ "inverted" primary creep occurs (17).

When the effective stress ($\sigma*$) slightly exceeds the athermal plateau stress (σ_c), a large increase in the stress exponent (n) occurs. This causes very large increases in strain rate for small stress increases, with a correspondingly large increase in the work hardening rate. The net result is that $\sigma*$ stays essentially equal to σ_c. In Zircaloy $\sigma_c = 2 \times 10^{-3}$ E (Figure 4). A strain increment by this process $\Delta\varepsilon_a$ causes an increase in internal stress $\Delta\sigma_i = A\Delta\varepsilon_a$.

3.1.2 Grain- or Phase-Boundary Sliding, $\dot{\varepsilon}_{gb}$

The creep strain due to grain boundary sliding is represented by an expression of the form

$$\dot{\varepsilon}_{gb} = F \left(\frac{\sigma_a}{d}\right)^m \exp\left(\frac{-Q}{T}\right) \qquad \ldots 7$$

where d is the grain size in μm. The constants are given table 3.

TABLE 3 CONSTANTS FOR EQUATION 7 FOR $\dot{\varepsilon}$ IN s^{-1}, σ IN MPa T IN K, AND MODULUS, μ, in MPa

Constant	α-phase	α+β-phase
F	$6.34 \times 10^6/\mu^2$	0.3
m	2.0	1.9
Q	9431	6039

3.1.3 Transformation Strain, $\dot{\varepsilon}_{tr}$

During the transition between α and β-phase Zircaloy, the crystal lattice undergoes a 10% strain at the interface between the two phases. On transforming to the β, the equivalent strain rate averaged over the β-phase fraction present is

$$\dot{\varepsilon}_f = 0.1\ \dot{f}\beta/f\beta \qquad \ldots 8$$

On transforming to the α, the equivalent strain rate is

$$\dot{\varepsilon}_f = 0.1\ \dot{f}\alpha/f\alpha \qquad \ldots 9$$

It should be noted that $\dot{f}\alpha = -\dot{f}\beta$ during the transformation where fα and fβ are the volume fractions of α and β respectively. An effective stress (σ_*) corresponding to ε_f (equation 6) is used in the work hardening/recovery expression for $\dot{\sigma}_i$ (equation 5) to calculate the change in dislocation structure occurring during the transformation.

The equivalent strain rate, $\dot{\varepsilon}_f$, occurs isotropically and in a polycrystalline material produces no macroscopic strain. However, when an applied stress is present, transformation strains occur preferentially in the direction of the applied stress and a

macroscopic strain rate results. This transformation strain rate in s^{-1} is given by

$$\dot{\varepsilon}_{tr} = 2.4 \times 10^{-3} \dot{f} \sigma_a \qquad \ldots 10$$

with stress in MPa and f equal to the absolute rate of transformation.

3.1.4 Total Strain Rate, $\dot{\varepsilon}$

The total creep rate at any time during the transient is found as the sum of the separate strain components.

$$\dot{\varepsilon} = \dot{\varepsilon}_d + \dot{\varepsilon}_u + \dot{\varepsilon}_{gb} + \dot{\varepsilon}_{tr} \qquad \ldots 11$$

When the Zircaloy is a mixture of a weak and a strong component - during recrystallization and in the two phase field - both components are assumed to have equal dislocation creep rates and the applied stress is distributed on a volumetric basis.

3.2 Microstructural Models

3.2.1 Recrystallization (Annealing)

For temperatures greater than 700 K, dislocations are removed by recrystallization. The rate of recrystallization is modelled by the expression

$$\dot{R} = -1.47 \times 10^{21} \exp\left\{\frac{-46753}{T}\right\} R \qquad \ldots 12$$

where R is the unrecrystallized volume fraction, $\dot{R}$ is in s^{-1} and T is absolute temperature (K).

3.2.2 α-phase Fraction

The variation of phase distribution with temperature (Figure 2) is taken from the equilibrium phase distribution [35,36]. Changes in the phase distribution due to oxygen addition and rate of heating and cooling are currently not represented.

3.2.3 Grain Size Variation

Grain size variation with temperature (Figure 2) is evaluated from metallographic examination of fuel sheaths after heating to various temperatures. An analytical expression for

grain growth as a function of time and temperature is under development.

4. MODEL CALIBRATION AND VERIFICATION

In the pressurized tube tests [6,8] are all of the creep and microstructural components described in Section 3 are present. Comparison with these tests (Figure 3)provides verification of the multi-component creep model over a full range of conditions. In such tests, the diffusional and transitional creep components are normally dominant at low strains and strain rates, while large strains and strain rates are dominated by dislocation creep. Wherever possible, the multi-component creep model was calibrated against data sources independent of those used for verification.

4.1 Dislocation Creep (Section 3.1.1)

The work hardening/recovery model for dislocation creep was formulated and tested using isothermal, constant plastic strain rate data for Zr-Sn alloys [15]. The model was calibrated for Zircaloy tubes using data from isothermal, uniaxial tests [16,17]. The plateau stress for athermal glide, 0.2% of Young's modulus, Figure 4, was obtained from a review of data in the open literature.

4.2 Grain Boundary Sliding (Section 3.1.2)

The grain boundary sliding component is negligible for α-phase or transformed β because of the large grain size. In the $\alpha+\beta$ phase field, the expression was calibrated against the uniaxial test of Clendening [24]. The expression developed by Coleman [25] for grain boundary sliding in large-grain, crystal bar zirconium is used in the α-phase. This creep component has not been verified against independent tests although it has been studied by other workers [26-28].

4.3 Transformation Strain (Section 3.1.3)

The expression for transformation strain was formulated and calibrated against pressurized tube tests [6]. It was verified using data from the U.K. [28]. Both data sets are shown in Figure 5.

4.4 Recrystallization (Section 3.2.1)

The first order chemical rate equation, assumed to describe recrystallization in Zircaloy, was fitted to isothermal annealing data from GE [29] and verified for high heating rates by Hunt [30]. Comparison of the model with both sets of data is shown in Figure 6.

4.5 Transformation Hardening (Section 3.1.3)

Figure 7 displays the type of "inverted" primary creep in the β-phase [17] which work hardening during the α→β transformation produces. The hardening expression is derived from fundamental considerations and this comparison verifies the model [31].

5. CREEP STRAIN CALCULATION

The rates of change of sheath temperature, differential pressure or axial load (Sec. 2), microstructural variables (Sec. 3) and the creep rates (Sec. 3) form a set of simultaneous differential equations which are solved by numerical integration (trapezoidal). Increments in the variables are limited to ensure accuracy of the integration. The anisotropic factors are altered to reflect changes in microstructure (Table 1) as the transient simulation progresses.

The form of the numerical integration can be illustrated by the creep strain calculation. The change in total plastic strain during any time step (Δt) is restricted to 10^{-3}. The plastic strain increment ($\Delta\varepsilon$) formed during Δt is found as

$$\Delta\varepsilon = \tfrac{1}{2}(\dot{\varepsilon}'+\dot{\varepsilon})\ t \qquad \ldots 13$$

where $\dot{\varepsilon}$ and $\dot{\varepsilon}'$ are the initial and final total creep rates respectively. The next allowable time step in the integration ($\Delta t'$) is set as

$$\Delta t' = 10^{-3}/\dot{\varepsilon}' \qquad \ldots 14$$

A set of allowable time steps is calculated, as in equation (14), for each process. The smallest time step of the set is used as the actual time step for the following integration interval.

The principal plastic strain increments ($\Delta\varepsilon_\theta, \Delta\varepsilon_r, \Delta\varepsilon_z$) are calculated from the equivalent plastic strain increment (Δt) using the flow rule for anisotropic materials [13]

$$\begin{aligned}
\Delta\varepsilon_\theta &= \frac{\Delta\varepsilon}{\sigma_e}\{H(\sigma_\theta-\sigma_r)-F(\sigma_z-\sigma_\theta)\} \\
\Delta\varepsilon_r &= \frac{\Delta\varepsilon}{\sigma_e}\{G(\sigma_r-\sigma_z)-H(\sigma_\theta-\sigma_r)\} \\
\Delta\varepsilon_z &= \frac{\Delta\varepsilon}{\sigma_e}\{F(\sigma_z-\sigma_\theta)-G(\sigma_r-\sigma_z)\}
\end{aligned} \qquad \ldots 15$$

These principal strain increments are accumulated to obtain the total principal strain at any time.

The stresses and strains calculated by the program are true values as opposed to engineering values. The dimensions used to evaluate the principal stresses in equations (2) and (3) are instantaneous values, i.e. $r=r_o \exp(\varepsilon_\theta)$ and $t=t_o \exp(\varepsilon_r)$ where r_o and t_o are initial mean radius and wall thickness respectively.

VI. LIMITATIONS

As the creep model is designed to represent high-temperature behaviour, application is limited to situations in which the sheath temperature is quickly increased to greater than 700 K while negligible creep strain occurs.

The effect of oxygen on mechanical properties due to the zirconium/steam reaction at high temperatures [32] is currently not accounted for. Simulations of tube tests are restricted to tests in an inert atmosphere. Oxygen either retards sheath creep or leaves it unchanged [33,34] and inclusion of oxygen effects into the model is in progress.

The variation of grain size with temperature is not calculated explicitly (Fig.2). The variation used in the model was evaluated from metallographic examination of Zircaloy tubing after a variety of heating cycles. Starting material with a larger grain size could show reduced plastic strain during transients.

Transformation from α to β is represented using the equilibrium phase distribution as a function of temperature (Fig.2). A transformation kinetics model is being developed because the phase transformation is retarded on heating and cooling through the two-phase region. Significant delay can occur for cooling rates as low as 5 K/s [35,36]. As creep rates are sensitive to temperature and phase distribution, creep strains could be predicted incorrectly under some conditions.

The model contains no representation of kinematic (directional) work hardening. Thus, strain rates would be overpredicted after a rapid reduction in load or a load reversal. A kinematic hardening model compatible with the internal stress (σ_i) formulation is currently being developed.

It is always necessary to supply the creep model with an appropriate initial value of σ_i. Before recrystallization (Fig.6), the initial dislocation structure of the tube has a pronounced effect on dislocation creep (Sec. 3.1.1). This dislocation structure depends upon the fabrication route and history (thermal, irradiation) prior to testing. In the comparison of the creep model to the pressurized tube data (Fig. 3), an

initial internal stress of 54 MPa was assumed to represent the prior history of the unirradiated tubing used.

VII. INPUT/OUTPUT

Program input and output is in SI units [37]. The pressure and sheath temperature history for the duration of the transient is supplied as input. Linear interpolation in these histories is used to obtain boundary conditions. The operating mode of the program can be selected to treat arbitrary transient test conditions as well as simulating standard mechanical tests.

VII.1 Input

Card 1 FORMAT(2A10)

ITYPE - AXIAL, isothermal,constant load,uniaxial
- UNIAXIAL, variable temperature and load, uniaxial
- BALLOON, constant pressure, biaxial
- VOID, constant moles of gas, biaxial
- LOCA, arbitrary transient simulation, biaxial

IMAT - ASRECEIVED, as-received Zircaloy
- ALPHA, α-annealed
- BETA, β-annealed.

Card 2 FORMAT(8A10)

IMAG( ) - alphanumeric title card

Card 3 Free Format*

SHOD - sheath OD (mm)
SHWALL- sheath wall thickness (mm)
SHLEN - sheath length (mm)
PXL - initial internal gas pressure or axial load (MPa)
VOLI - internal volume available for gas (mm^3)
PLAS - initial plastic strain
SINT - initial internal stress at room temperature (MPa)
PLEN - connected gas reservoir at constant temperature (mm^3/K).

Card 4 Free Format

HILL( ) F,G and H anisotropic factors (Sec. 2) for as-received, α-annealed and β-annealed Zircaloy sheath respectively.

Card 5 Free Format

These are history cards whose content depends upon the

*free format requires all values to be given even if zero.

execution mode (ITYPE).

a) ITYPE=AXIAL
SEC( ) - time (s)
TSH( ) - sheath temperature (°C)
SPLIT( )- number of equally spaced printouts between SEC(I-1) and SEC(I).

b) ITYPE=UNIAXIAL
SEC( ) -
TSH( ) -
PEXT( ) - axial stress (MPa)
SPLIT( )-

c) ITYPE=BALLOON
SEC( ) -
TSH( ) -
SPLIT( )-

d) ITYPE=VOID
SEC( ) -
TSH( ) -
PEXT( ) - external pressure (MPa)
SPLIT( )-

e) ITYPE=LOCA
SEC( ) -
TSH( ) -
TGAS( ) - temperature of internal gas (°C)
PEXT( ) - external pressure (MPa)
SPLIT( )-

As many card 5's as required (maximum 50) to describe history. The last card must contain all zeros.

VII.2 Output

Output consists of a labelled summary of the input data plus a tabular history of results (Fig.8). Output variables have the following meaning:

TIME	- time
TEMP	- sheath temperature
URX	- fraction of material unrecrystallized (Sec. 3.2.1).
ALPHA	- fraction of material in α-phase
SIGO	- internal stress (equivalent) in unrecrystallized fraction (Sec. 3.1.1)
SIGA	- internal stress (equivalent) in α-phase fraction

SIGB	- internal stress (equivalent) in β-phase fraction
GENERALIZED STRESS	- equation (1)
ATH	- athermal strain component (Sec. 3.1.1).
GB	- diffusional creep component (Sec. 3.1.2)
DIS	- dislocation creep component (Sec. 3.1.1)
TRANS	- transition creep component (Sec. 3.1.3)
TOT	- total creep strain (Sec. 3.1.4)
PREDICTED STRAIN	- true axial strain in uniaxial tests - true tangential strain (diametral expansion) in biaxial simulations

VIII. ACKNOWLEDGEMENTS

We would like to thank S.R. MacEwen for many helpful discussions during development of this model and C.E.L. Hunt, S. Sagat, W.R. Clendening and C.E. Coleman for permission to use their unpublished data.

References

1. Hobson, D.O., Osborne, M.F., and Parker, G.W., Comparison of Rupture Data from Irradiated Fuel Rods and Unirradiated Cladding, Nuc. Tech., 11 (1971), p.479.

2. Emmerich, K.M., Juenke, E.F., and White, J.F., Failure of Pressurized Zircaloy Tubes During Thermal Excursions in Steam and Inert Atmospheres, ASTM STP 458 (1969) p.252.

3. Roll, J.B., Performance of Zircaloy Clad Fuel Rods During a Simulated Loss-of-Coolant Accident - Single Rod Tests, WCAP-7379, Vol.II, Westinghouse Electric Corporation, (1969).

4. Waddell, R.D. and Rittenhouse, P., High-Temperature Burst Strength and Ductility of Zircaloy Tubing, ORNL-TM-3289, Oak Ridge National Laboratoray, (1971).

5. Emery, A.D., Scott, D.B., and Stewart, J.R., Effects of Heating Rate and Pressure on Expansion of Zircaloy Tubing During Sudden Heating Conditions, Nucl. Tech., 11 (1971), p.474.

6. Hardy, D.G., High Temperature Expansion and Rupture Behaviour of Zircaloy Tubing, National Topical Meeting on Water Reactor Safety, Salt Lake City, USA, (1973).

7. Clendening, W.R., Primary and Secondary Creep Properties for Zircaloy Cladding at Elevated Temperatures of Interest in Accident Analysis, 3rd SMIRT Conference, London, England (1975).

8. Hunt, C.E.L., and Foote, D.E., ASTM STP 683 (1977), p.51.

9. Busby, C.C. and White, L.S., Some High Temperature Mechanical Properties of Internally Pressurized Zircaloy-4 Tubing, WAPD-TM-1243 (1976).

10. Clay, B.D. and Redding, G., Creep Rupture Properties of α-phase Zircaloy-4 Cladding Relevant to the Loss-of-Coolant Accident, CEGB Report RD/B/N3187 (1975).

11. Clay, B.D. and Stride, R., Creep Rupture Properties of Zircaloy-2 Tubes from 1000°C to 1200°C, CEGB Report RD/B/N3782 (1977).

12. Sills, H.E. and Holt, R.A., Predicting High-Temperature Transient Deformation from Microstructural Models, 4th International Conference on Zirconium in the Nuclear Industry, Stratford-upon-Avon, U.K., (1978).

13. Hill, R., Proc. Roy. Soc. A, 193 (1948) p.281.

14. Ashby, M.F., Acta Met., 20 (1972), p.887.

15. Luton, M.J., High Temperature Deformation of Zirconium and Zirconium Tin Alloys, Ph.D. Thesis, McGill University, (1970).

16. Holt, R.A. and Sills, H.E., A Mathematical Model for Transient Deformation of Alpha Zirconium-Tin Alloys, ANS Trans., 27 (1977), p.295.

17. Holt, R.A., Model for "Inverted" Primary Creep in β-phase Zircaloy-4 Fuel Sheathing, ANS Trans., 27 (1977), p.294.

18. Hertier, B., Luton, M.J., and Jonas, J.J., Metal Science, 8 (1974), p.41.

19. Ibrahim, E.F., Private Communication.

20. Hardy, D.G., Irradiation Effects in Structural Materials for Nuclear Applications, ASTM STP 478 (1970), p.215.

21. Jenson, J.A. and Beckofen, W.A., Can. Met. Quart., 11 (1972), p.39.

22. Shohen, F.R. et al, Batelle Memorial Institute, Report BMI 1168 (1957).

23. Miller, A.K. and Sherby, O.D., Fifth Quarterly Progress Report, Development of MAT MOD, Electric Power Research Institute, Project #RP-4561-1, (1976).

24. Clendening, W.R., Private Communication.

25. Coleman, C.E., Private Communication.

26. Holm, K., Embury, J.D., and Purdy, G.R., Acta Met., 25 (1977), p.1191.

27. Gittus, J.H., High-Temperature Deformation of Two-Phase Structures, Phil. Trans. R. Soc. Lond. A, 288 (1978) p.121.

28. Jones, P.M., Gittus, J.H. and Hindle, E.D., TRG Report 2901(S), UKAEA (1976).

29. Lee, D., J. Nucl. Mat., 37 (1970), p.159.

30. Hunt, C.E.L., Private Communication.

31. Sagat, S. and Foote, D.E., Private Communication

32. Urbanic, V.F., and Heidrick, T.R., High Temperature Oxidation of Zircaloy-2 and Zircaloy-4 in Steam, Atomic Energy of Canada Limited, Report AECL-6149 (1978).

33. Rizkalla, A.S., Holt, R.A., and Jonas, J.J., The Effect of Oxygen on the Deformation of Zircaloy-4 at Elevated Temperatures, 4th International Conference on Zirconium in the Nuclear Industry, Stratford-upon-Avon, U.K., (1978).

34. Burton, G., Donaldson A.T. and G.L. Reynolds, The Interaction of Oxidation and Creep in Zircaloy-2, CEGB Report RD/B/N4280, (1978).

35. Holt, R.A., J. Nuc. Mat., 25 (1970) p.322.

36. Holt, R.A., J. Nuc. Mat., 47 (1973) p.262.

37. Canadian Standards Association, Canadian Metric Practice Guide, CAN3-Z234.1-76 (1976).

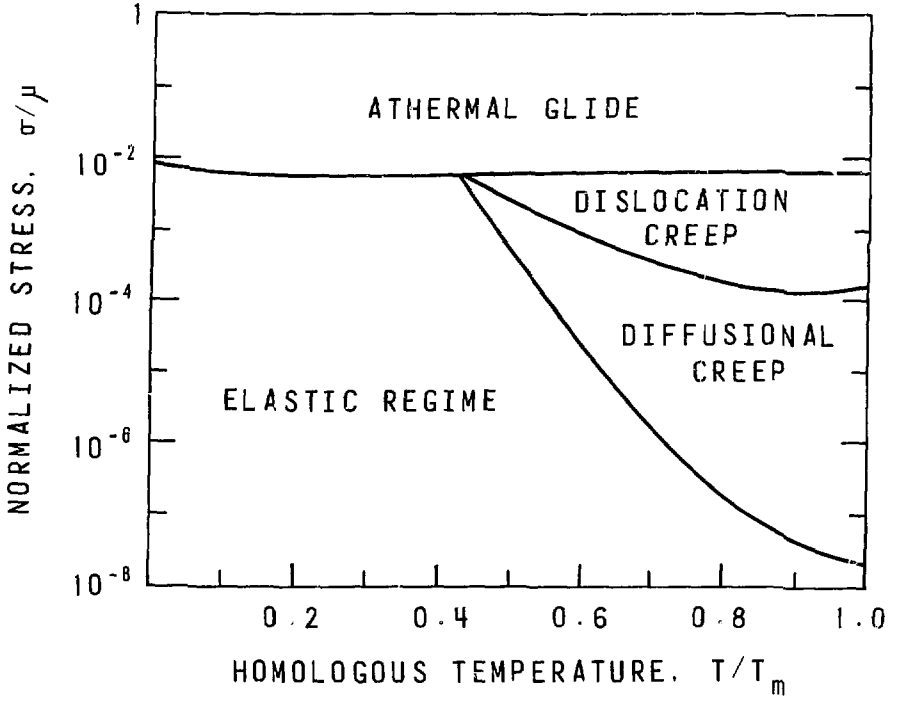

DEFORMATION MAP SHOWING TYPICAL STRESS/TEMPERATURE DOMAINS WHERE DIFFERENT STRAIN PROCESSES DOMINATE (μ, SHEAR MODULUS; T_m, MELTING TEMPERATURE)

FIGURE 1

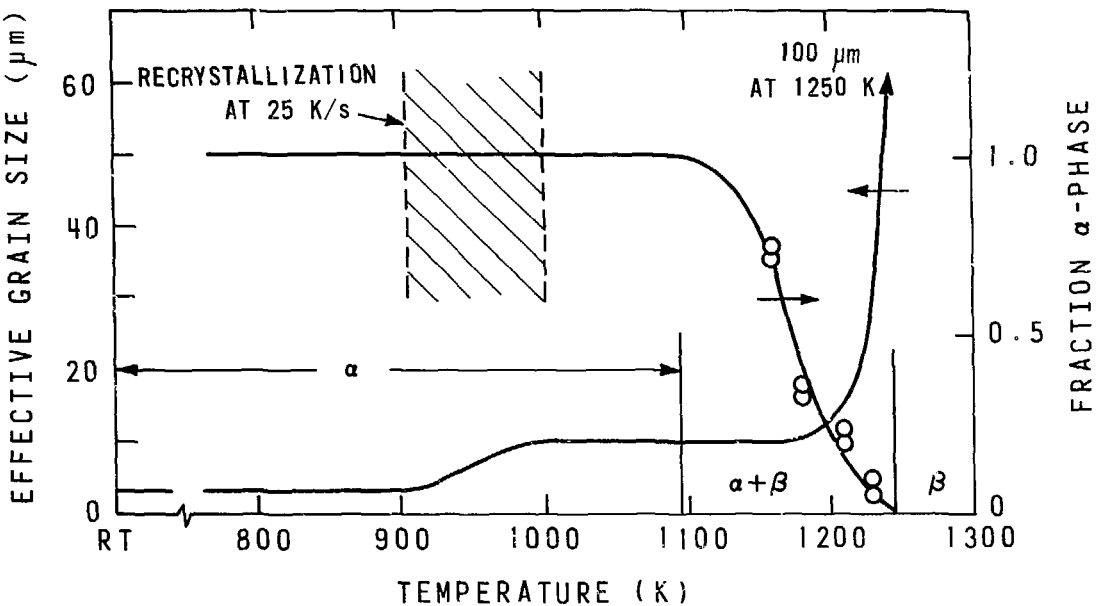

VARIATION WITH TEMPERATURE OF GRAIN SIZE AND α-PHASE FRACTION OF COLD-WORKED ZIRCALOY [35,36] AS USED IN MODEL

FIGURE 2

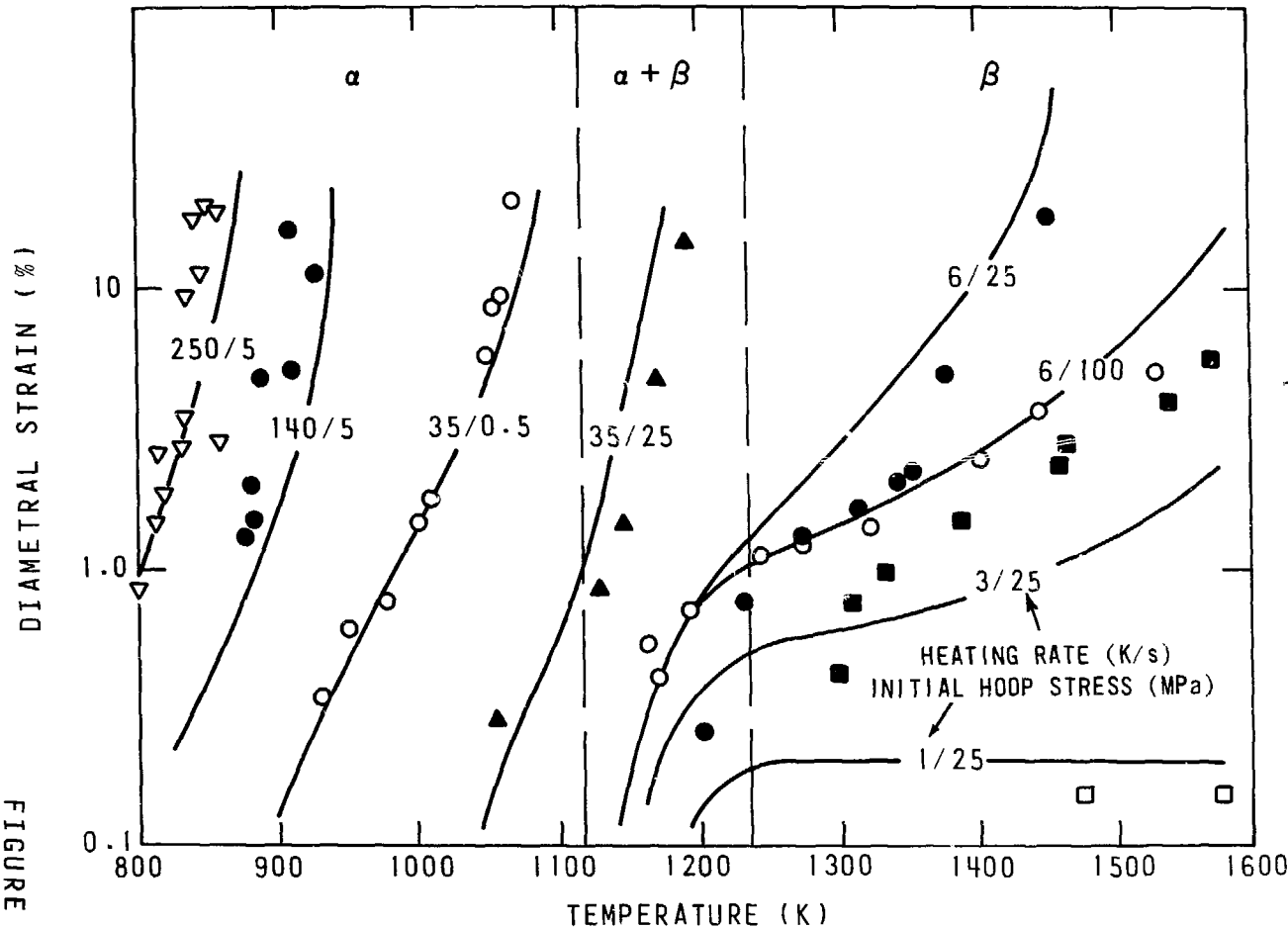

FIGURE 3

TRANSIENT STRAIN MODEL COMPARISON WITH CONSTANT PRESSURE. CONSTANT HEATING RATE TESTS ON ZIRCALOY-4 SHEATHING [6,8]

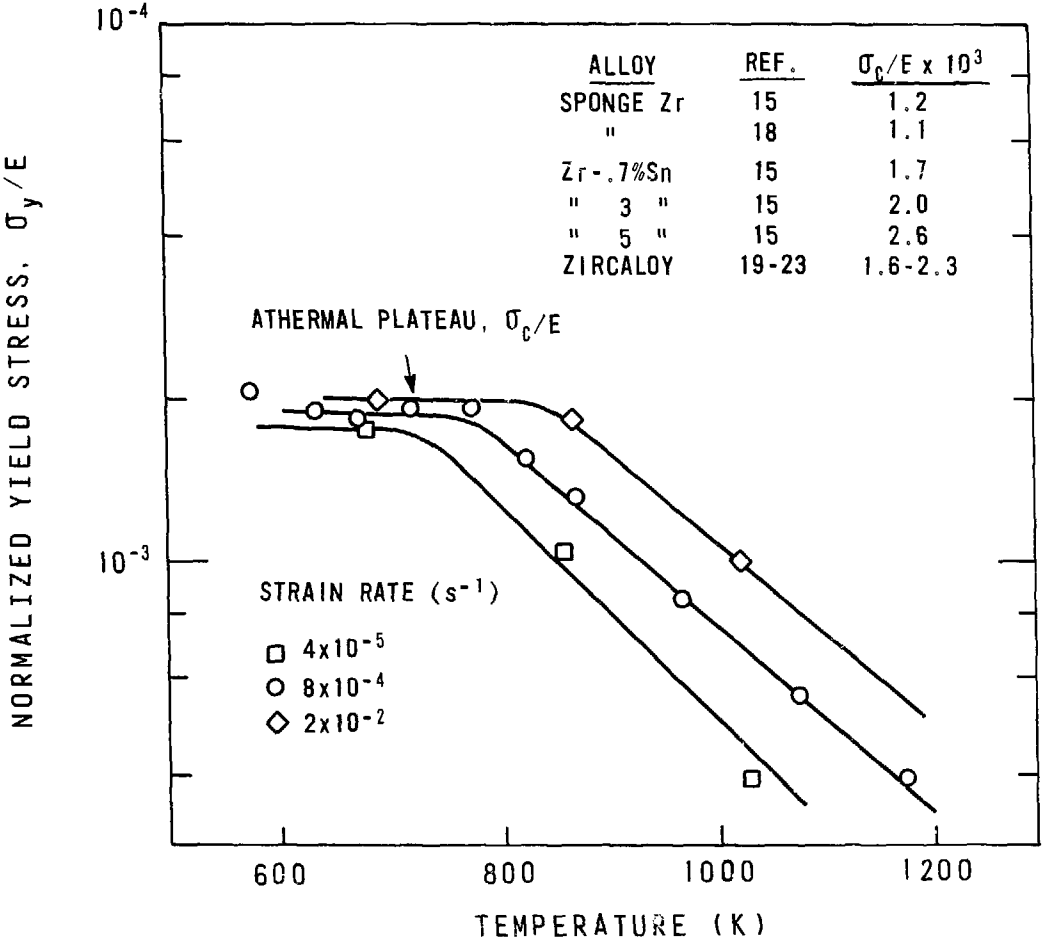

FIGURE 4

YIELD STRESS OF ZIRCONIUM AS A FUNCTION OF STRAIN RATE AND TEMPERATURE SHOWING ATHERMAL/THERMAL TRANSITION [23] CRITICAL STRESS VALUES FOR SOME ZIRCONIUM ALLOYS LISTED.

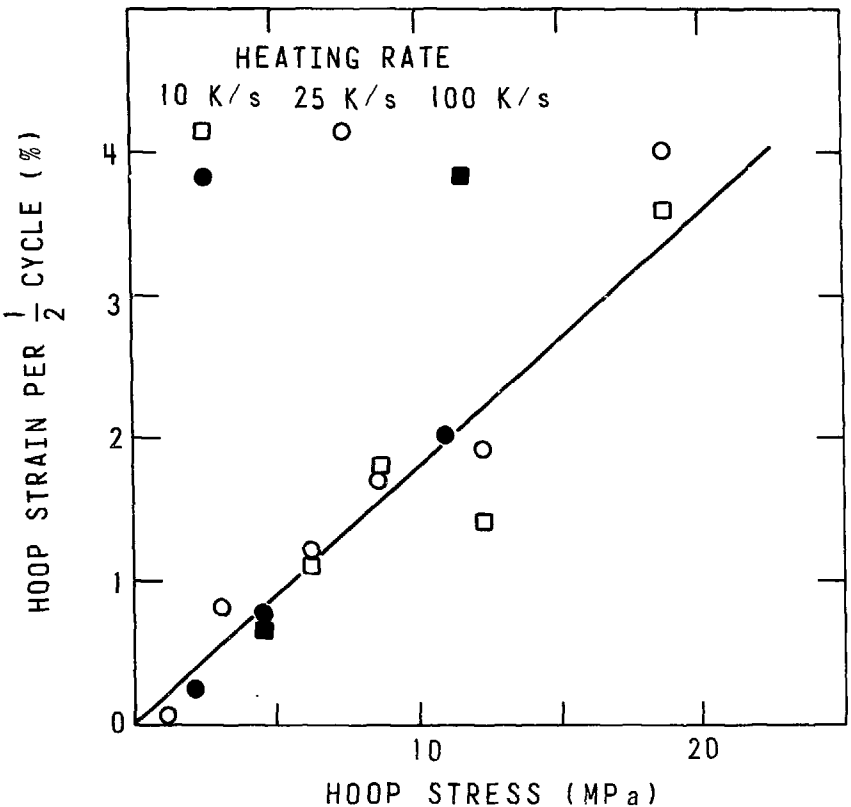

PLASTIC STRAIN INCREMENT IN ZIRCALOY ON PASSING ONCE THROUGH THE $\alpha+\beta$ PHASE FIELD UNDER STRESS. OPEN SYMBOLS, CRNL [6.8]; CLOSED SYMBOLS, SPRINGFIELDS [28].

FIGURE 5

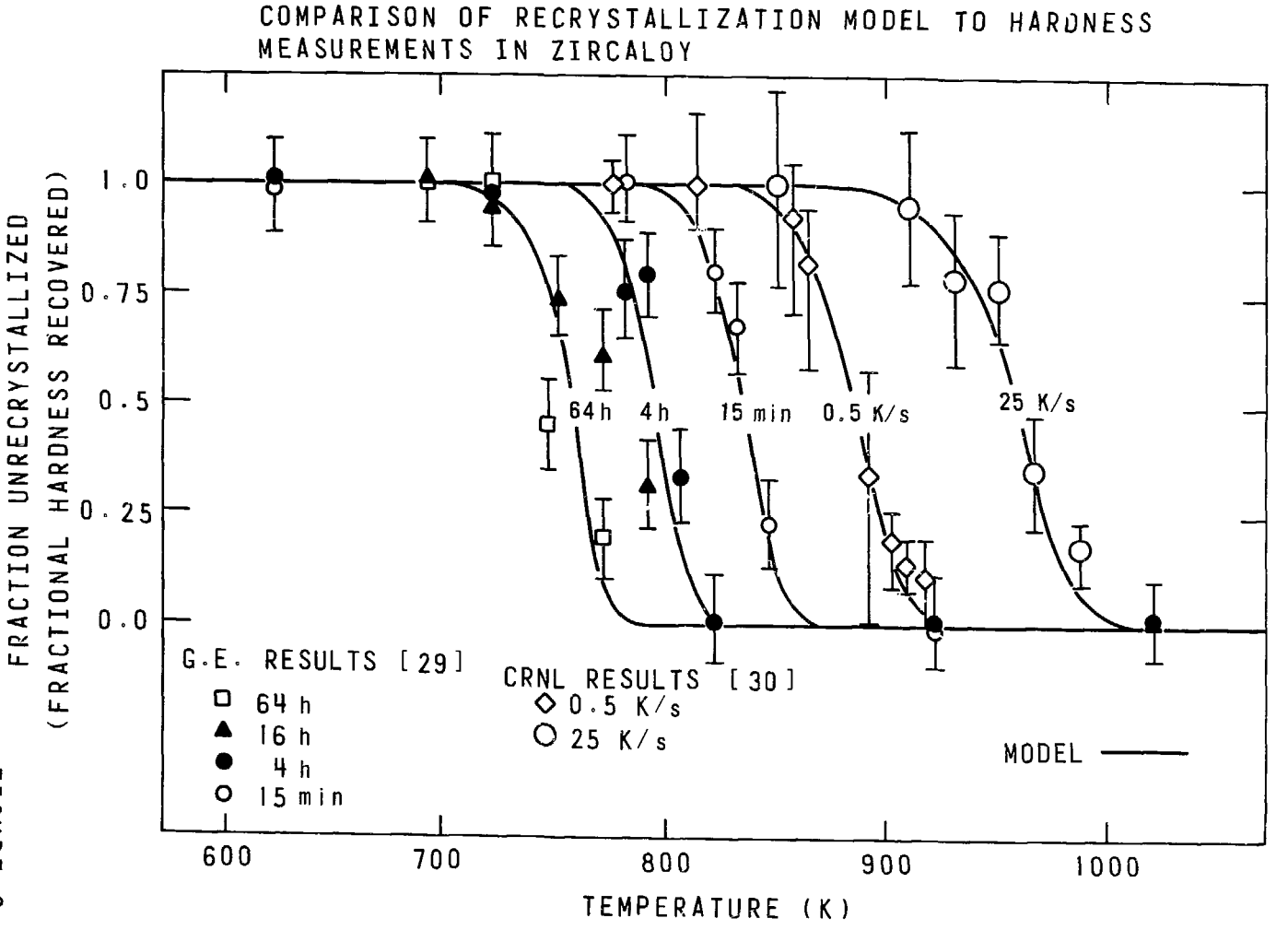
COMPARISON OF RECRYSTALLIZATION MODEL TO HARDNESS MEASUREMENTS IN ZIRCALOY
FRACTION UNRECRYSTALLIZED (FRACTIONAL HARDNESS RECOVERED)
1.0
0.75
0.5
0.25
0.0
600
700
800
900
1000
TEMPERATURE (K)
64 h
4 h
15 min
0.5 K/s
25 K/s
G.E. RESULTS [29]
64 h
16 h
4 h
15 min
CRNL RESULTS [30]
0.5 K/s
25 K/s
MODEL

FIGURE 6

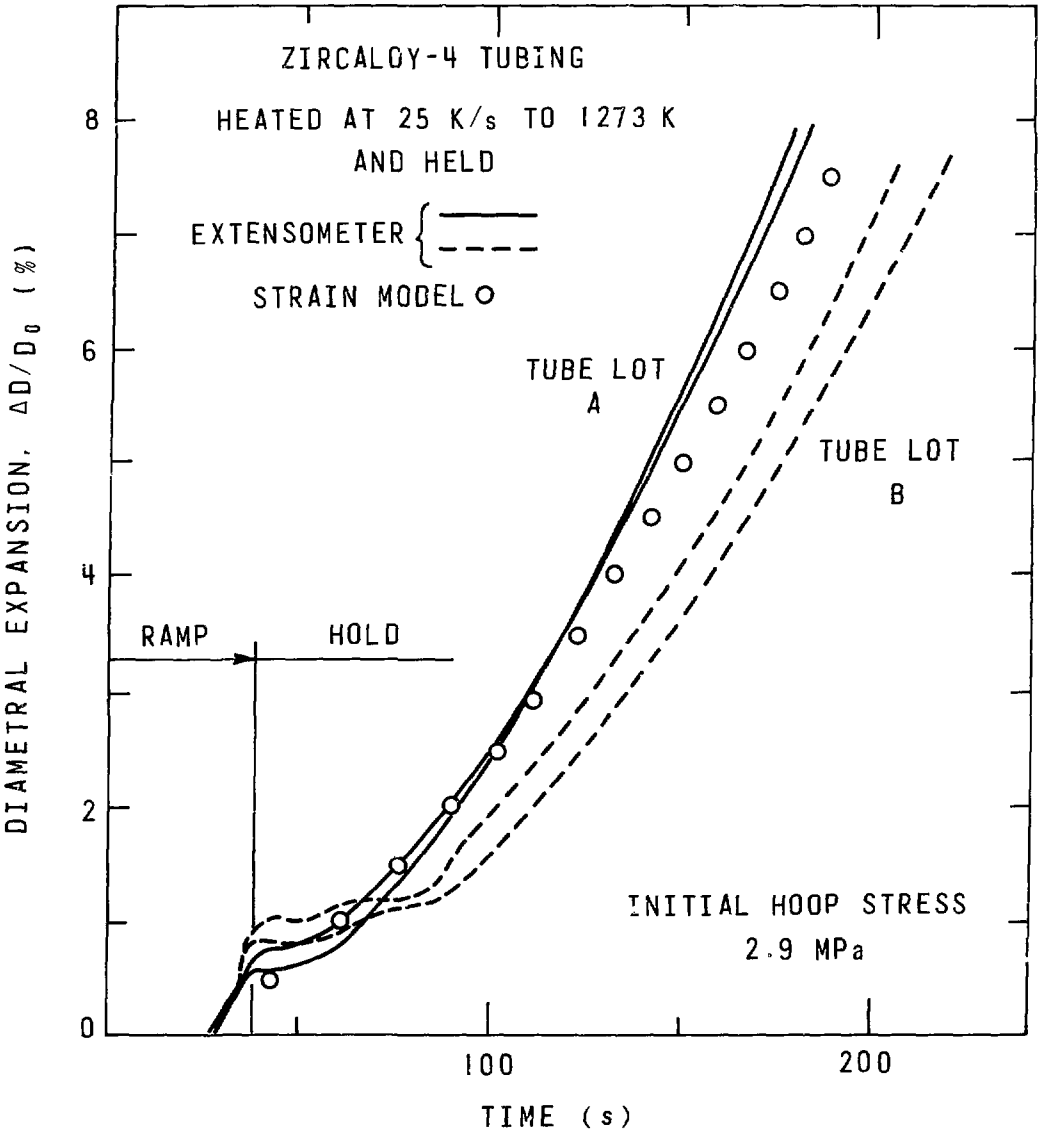

DEFORMATION OF ZIRCALOY-4 SHEATHING AT CONSTANT INTERNAL PRESSURE SHOWING "INVERTED" PRIMARY CREEP IN THE β-PHASE

FIGURE 7

BALLOON
ASRECEIVED

SIMULATION OF RAMP AND HOLD TEST

SHEATH OD (MM) = 17.248
SHEATH WALL THICKNESS (MM) = 0.490
SHEATH INTERNAL LENGTH (MM) = 489.200
AXIAL STRESS OR GAS PRESSURE (MAPA) = 0.172
INTERNAL VOID VOLUME (MM3) = 101682.00
INITIAL PLASTIC STRAIN = 0.00000
INITIAL INTERNAL STRESS (MAPA) = 54.30
PLENUM VOID (MM3/K) = 0.000

ANISOTROPIC FACTORS	F	G	H
AS RECEIVED	0.773	0.532	0.195
ALPHA ANNEALLED	0.956	0.322	0.222
BETA ANNEALLED	0.572	0.418	0.510

HISTORY CARDS

TIME (S)	SHEATH TEMP. (CEL)	GAS TEMP. (CEL)	EXT. PRESS (MAPA)	NUMBER OF PRINTS
0.00	20.00	0.00	0.00	1.
24.00	620.00	0.00	0.00	1.
28.00	720.00	0.00	0.00	10.
31.20	800.00	0.00	0.00	1.
39.20	1000.00	0.00	0.00	8.
40.00	1000.00	0.00	0.00	1.
200.00	1000.00	0.00	0.00	16.

FIGURE 8A

BALLOON
ASRECEIVED

SIMULATION OF RAMP AND HOLD TEST

TIME (S)	TEMP (CEL)	URX (%)	ALPHA (%)	--INTERNAL STRESS--- SIGO (MAPA)	SIGA (MAPA)	SIGB (MAPA)	GENERALIZED STRESS (MAPA)	----------GENERALIZED STRAIN---------- ATH (%)	GB (%)	DIS (%)	TRANS (%)	TOT (%)	PREDICTED STRAIN (%)
0.00	20.00	100.0	100.0	54.30	0.00	0.00	2.13	0.00	0.00	0.00	0.00	0.00	0.00
24.00	620.00	98.3	100.0	34.60	0.00	0.00	2.13	0.00	0.00	0.00	0.00	0.00	0.00
24.40	630.00	97.0	100.0	34.28	0.00	0.00	2.13	0.00	0.00	0.00	0.00	0.00	0.00
24.80	640.00	94.6	100.0	33.95	0.00	0.00	2.13	0.00	0.00	0.00	0.00	0.00	0.00
25.20	650.00	90.7	100.0	33.62	0.00	0.00	2.13	0.00	0.00	0.00	0.00	0.00	0.00
25.60	660.00	84.1	100.0	33.29	0.00	0.00	2.13	0.00	0.00	0.00	0.00	0.00	0.00
26.00	670.00	73.9	100.0	32.96	0.00	0.00	2.14	0.00	0.00	0.00	0.00	0.00	0.00
26.40	680.00	59.2	100.0	32.63	0.00	0.00	2.14	0.00	0.00	0.00	0.00	0.00	0.00
26.80	690.00	40.6	100.0	32.31	0.00	0.00	2.15	0.00	0.00	0.00	0.00	0.00	0.00
27.20	700.00	21.5	100.0	31.98	0.00	0.00	2.16	0.00	0.00	0.00	0.00	0.00	0.00
27.60	710.00	7.3	100.0	31.65	0.00	0.00	2.17	0.00	0.00	0.00	0.00	0.00	0.00
28.00	720.00	1.1	100.0	31.32	0.00	0.00	2.17	0.00	0.00	0.00	0.00	0.00	0.00
31.20	800.00	0.0	100.0	0.00	0.00	0.00	2.17	0.00	0.00	0.00	0.00	0.00	0.00
32.20	825.00	0.0	98.2	0.00	0.00	0.30	2.26	0.00	0.00	0.00	0.00	0.00	0.00
33.20	850.00	0.0	94.3	0.00	0.00	1.06	2.56	0.00	0.01	0.00	0.02	0.03	0.03
34.20	875.00	0.0	83.4	0.00	0.00	1.07	2.57	0.00	0.02	0.00	0.09	0.11	0.10
35.20	900.00	0.0	50.8	0.00	0.00	1.04	2.57	0.00	0.03	0.00	0.29	0.32	0.29
36.20	925.00	0.0	24.1	0.00	0.01	0.93	2.58	0.00	0.03	0.00	0.46	0.49	0.44
37.20	950.00	0.0	8.7	0.00	0.03	0.85	2.58	0.00	0.03	0.00	0.55	0.59	0.53
38.20	975.00	0.0	0.0	0.00	0.00	0.80	2.58	0.00	0.03	0.02	0.60	0.65	0.58
39.20	1000.00	0.0	0.0	0.00	0.00	0.80	2.58	0.00	0.03	0.04	0.60	0.67	0.60
40.00	1000.00	0.0	0.0	0.00	0.00	0.79	2.58	0.00	0.03	0.06	0.60	0.69	0.62
50.00	1000.00	0.0	0.0	0.00	0.00	0.73	2.60	0.00	0.04	0.32	0.60	0.96	0.85
60.00	1000.00	0.0	0.0	0.00	0.00	0.66	2.61	0.00	0.04	0.63	0.60	1.27	1.11
70.00	1000.00	0.0	0.0	0.00	0.00	0.61	2.63	0.00	0.04	0.99	0.60	1.62	1.42
80.00	1000.00	0.0	0.0	0.00	0.00	0.57	2.64	0.00	0.04	1.39	0.60	2.03	1.77
90.00	1000.00	0.0	0.0	0.00	0.00	0.53	2.67	0.00	0.04	1.83	0.60	2.48	2.16
100.00	1000.00	0.0	0.0	0.00	0.00	0.50	2.69	0.00	0.04	2.33	0.60	2.97	2.59
110.00	1000.00	0.0	0.0	0.00	0.00	0.48	2.71	0.00	0.04	2.86	0.60	3.51	3.05
120.00	1000.00	0.0	0.0	0.00	0.00	0.47	2.74	0.00	0.05	3.44	0.60	4.08	3.55
130.00	1000.00	0.0	0.0	0.00	0.00	0.46	2.77	0.00	0.05	4.05	0.60	4.70	4.09
140.00	1000.00	0.0	0.0	0.00	0.00	0.45	2.80	0.00	0.05	4.70	0.60	5.35	4.65
150.00	1000.00	0.0	0.0	0.00	0.00	0.45	2.84	0.00	0.05	5.39	0.60	6.05	5.25
160.00	1000.00	0.0	0.0	0.00	0.00	0.45	2.87	0.00	0.05	6.12	0.60	6.78	5.89
170.00	1000.00	0.0	0.0	0.00	0.00	0.45	2.91	0.00	0.06	6.89	0.60	7.55	6.56
180.00	1000.00	0.0	0.0	0.00	0.00	0.45	2.95	0.00	0.06	7.71	0.60	8.37	7.26
190.00	1000.00	0.0	0.0	0.00	0.00	0.45	3.00	0.00	0.06	8.58	0.60	9.24	8.02
200.00	1000.00	0.0	0.0	0.00	0.00	0.46	3.04	0.00	0.06	9.50	0.60	10.16	8.82

FIGURE 8b

ISSN 0067 - 0367

To identify individual documents in the series we have assigned an AECL- number to each.

Please refer to the AECL- number when requesting additional copies of this document

from

Scientific Document Distribution Office
Atomic Energy of Canada Limited
Chalk River, Ontario, Canada
K0J 1J0

Price $3.00 per copy

ISSN 0067 - 0367

Pour identifier les rapports individuels faisant partie de cette série nous avons assigné un numéro AECL- à chacun.

Veuillez faire mention du numéro AECL- si vous demandez d'autres exemplaires de ce rapport

au

Service de Distribution des Documents Officiels
L'Energie Atomique du Canada Limitée
Chalk River, Ontario, Canada
K0J 1J0

Prix $3.00 par exemplaire